

Simulating the Diffuse Neutrino Emission from the Milky Way with GALPROP

P. D. MARINOS ,¹ T. A. PORTER ,¹ G. P. ROWELL ,² I. V. MOSKALENKO ,¹ AND G. JÓHANNESSEN ,³

¹ *W. W. Hansen Experimental Physics Laboratory and Kavli Institute for Particle Astrophysics and Cosmology, Stanford University, Stanford, CA 94305, USA*

² *School of Physical Sciences, University of Adelaide, Adelaide, South Australia 5000, Australia*

³ *Science Institute, University of Iceland, IS-107 Reykjavik, Iceland*

ABSTRACT

We use the GALPROP cosmic ray (CR) propagation framework to model the diffuse neutrino and gamma-ray (γ -ray) emissions from the Galaxy. A collection of realistic bounding models are developed and predictions of the resulting neutrino and γ -ray signals are compared to the IceCube and LHAASO data up to PeV energies. We find that all the GALPROP models are consistent with the neutrino data within uncertainties. They are also consistent with expectations of neutrino emissions derived from LHAASO data when accounting for possible γ -ray point source contamination. The new models present state-of-the-art predictions for the VHE neutrino emissions from the Galaxy that may be used for future neutrino searches.

Keywords: Particle Astrophysics (96) — Cosmic Rays (329) — Diffuse radiation (383) — Interstellar Emissions (840) — Neutrino astronomy (1100)

1. INTRODUCTION

Cosmic rays (CRs) diffuse throughout the Milky Way (MW), interacting with the interstellar medium (ISM) and creating secondary CRs, gamma rays (γ -rays), and neutrinos. These CRs and γ -rays have been observed and studied for decades across many orders of magnitude in energy. However, the CR propagation and injection mechanisms, as well as the hadronic/leptonic fraction, remain unconstrained. With the recent neutrino detection of the Galactic plane by IceCube we have an additional multi-messenger dataset that can aid in constraining the propagation and injection of CRs within the MW.

IceCube is a cubic-kilometre detector of >1 TeV neutrinos located at the South Pole. Prior to 2023, IceCube had only detected two astrophysical sources of very-high-energy (VHE) neutrinos: the blazar TXS 0506+056 (IceCube Collaboration et al. 2018a,b), and the active galaxy NGC 1068 (IceCube Collaboration et al. 2022). The third and most recent detection of a VHE neutrino source was the Galactic plane (IceCube Collaboration et al. 2023). However, IceCube was not able to detect the MW in a blind search, relying on input models to define the expected neutrino signal from the Galaxy. The three input models used by IceCube are based on CR diffusion codes. One input, the ‘ π^0 ’ model, is based on a 13-year-old GALPROP result

(Ackermann et al. 2012) tuned only to CR data. The other two models are based on Kraichnan-diffusion models tuned to CR and γ -ray data (named ‘KRA $_{\gamma}$ ’) calculated with the DRAGON CR propagation code (Gaggero et al. 2015). All three input spatial templates resulted in a successful detection of the MW plane, from which IceCube was able to measure the Galactic neutrino flux. These neutrino flux measurements then represent the sum of the source and diffuse components.

While neutrinos have not yet been used as a proxy measurement for the Galactic CR density, the γ -ray emission has been used for decades in the MeV–GeV regime. Various γ -ray observatories have reported a detection of the diffuse/large-scale emission in the TeV regime. One of these, the LHAASO observatory, detects γ -rays in the energy range of 0.5–500 TeV. The pp collisions generating these γ -rays also create neutrinos with energies (E_{ν}) in the range of 0.25–250 TeV. As the LHAASO and IceCube energy ranges overlap, their observations are connected. These neutrino and γ -ray datasets can then be correlated to one another, and can be used as upper-limits to constrain the hadronic components of Galactic γ -ray models.

In this paper we use up-to-date versions of the GALPROP framework¹, with the neutrino flux being computed with the latest interaction cross sections from AAfrag202. Using the steady-state (i.e. time-independent) propagation models we compute the neu-

trino flux over a range of parameter configurations to provide a modelling uncertainty. We also compute the uncertainties and related neutrino limits from the LHAASO γ -ray observations and compare to our model predictions. Our state-of-the-art models are then compared to the Galactic flux observed by IceCube. We find that the GALPROP predictions lie within all upper and lower limits on the diffuse neutrino emission for both LHAASO and IceCube. We find that all of our model predictions are consistent with the range of current Galactic observations. We also provide model neutrino predictions in the 1–100 TeV energy range. All of our model data products and configuration files are provided in the online material.

2. MODEL SETUP

The GALPROP framework (Moskalenko & Strong 1998; Strong & Moskalenko 1998) is a CR propagation package with an extensive history of reproducing the local CR spectra, Galactic synchrotron emission, and \sim keV to TeV γ -ray emission (e.g. Strong et al. 2000; Moskalenko et al. 2002; Strong et al. 2004; Porter et al. 2008; Strong et al. 2011; Boschini et al. 2020). Recently we have shown that models based on GALPROP version 57 (Porter et al. 2022) can also reproduce the observed γ -ray emission in the TeV–PeV regime (Marinos et al. 2023, 2025) from the high-energy stereoscopic system (H.E.S.S.) Galactic plane survey (HGPS) and the large high-altitude air shower observatory (LHAASO). In this paper we extend the models used in Marinos et al. (2023, 2025) to include the predicted neutrino emission.

We construct the ISM with multiple components: the interstellar radiation field (ISRF), the Galactic magnetic field (GMF), the gas distribution, and the source distribution (i.e. where CRs are injected into the MW). For all distributions, we chose models with spiral-arm descriptions of the MW. For the ISRF we use the Robitaille et al. (2012) model (hereafter referred to as R12) as described by Porter et al. (2017), and for the GMF we use the Pshirkov et al. (2011) model (hereafter referred to as PBSS) as described by Orlando & Strong (2013). For the 3D molecular (H_2) and neutral ($H\,I$) gas densities we use the models developed by Jóhannesson et al. (2018), and references therein. Previous results from Marinos et al. (2023) found that the hadronic emission has a strong dependence on the chosen source distribution. To estimate uncertainty due to degeneracy in the source distributions we simulate over a range of models. Hence, we simulate over a range of source distributions to estimate the variance between them. We use distributions with disc-like and spiral-arm components (see Porter et al. 2017, and references therein). The models are referred to by the percentage contribution from the spiral arm component – e.g. SA50 has an equal relative contribution from each component. We simulate over three distributions: SA0, SA50, and SA100. To replicate the diffuse emission calculation method used by the

LHAASO collaboration (Cao et al. 2023) we also test a fourth method that takes the post-diffusion/propagated CR spectra at the Solar location from the SA50 model and applies it uniformly across the MW. We hereby refer to this model as ‘u50’.

For the CR injection and diffusion parameters we take the values from Marinos et al. (2023) (see their Table 1). The parameters are obtained following the procedure in Porter et al. (2017) and Jóhannesson et al. (2018). For each source distribution (and ISM gas model) the propagated CR spectra are fit to data from AMS-02 and *Voyager 1* (see Jóhannesson et al. 2019, and references therein). The force-field approximation is applied instead of the more advanced GALPROP/HeMod framework as we are focusing on energies above which the Solar modulation has a significant impact (Boschini et al. 2020). The MW is constructed with a non-linear spatial grid (tan spatial grid; Porter et al. 2022) with the spatial grid size around the solar location set to 7 pc. We use ten kinetic energy bins per decade ranging from $1\,GeV\,nuc^{-1}$ to $10\,PeV\,nuc^{-1}$ for the hadronic CR propagation, and five bins per decade ranging from 1 GeV to 1 PeV for the neutrino flux calculation. The neutrino skymaps are computed on a seventh-order HEALPix (Górski et al. 2005) isopixelisation, giving a pixel size of $27.5' \times 27.5'$. We simulate hadrons up to and including silicon.

CR observations in the TeV energy regime (e.g. DAMPE; An et al. 2019) show a spectral ‘bump’ (i.e. a hardening followed by a softening). This TeV bump is likely due to some local phenomenon, such as a nearby source or some reacceleration effect (e.g. Liu et al. 2019; Fang et al. 2020; Malkov & Moskalenko 2021; Malkov et al. 2024; Bhadra et al. 2025). However, the sharp breaks and a very thin transition between the excess in the outer Galaxy and a deficit in the inner Galaxy along the magnetic equator in the anisotropy map at 10 TV (Abeysekara et al. 2019) rule out the likely sources beyond \sim 10 pc (Malkov et al. 2024).

Previously, we performed the spectral tuning of the CRs at 100 GeV and extrapolated into the TeV range to prevent overfitting to a potentially local effect. Here we test over a range of CR injection indices to evaluate the sensitivity of the diffuse neutrino emission to the Galactic CR spectrum and to account for observational uncertainties in the >10 TeV CR flux. We take the previously used injection indices from Marinos et al. (2023) for rigidities $R > 266$ GV for protons ($\gamma_{2,p} \sim 2.35$) and helium ($\gamma_{2,He} \sim 2.3$) and vary both by ± 0.1 . The GALPROP propagated CR proton and helium spectra are shown in the Appendix in Figures 5 and 6. All our model parameter values are included within the configuration files supplied online.

2.1. Neutrino Calculations

We calculate the neutrino emissivity for CR proton and helium collisions with the hydrogen and helium

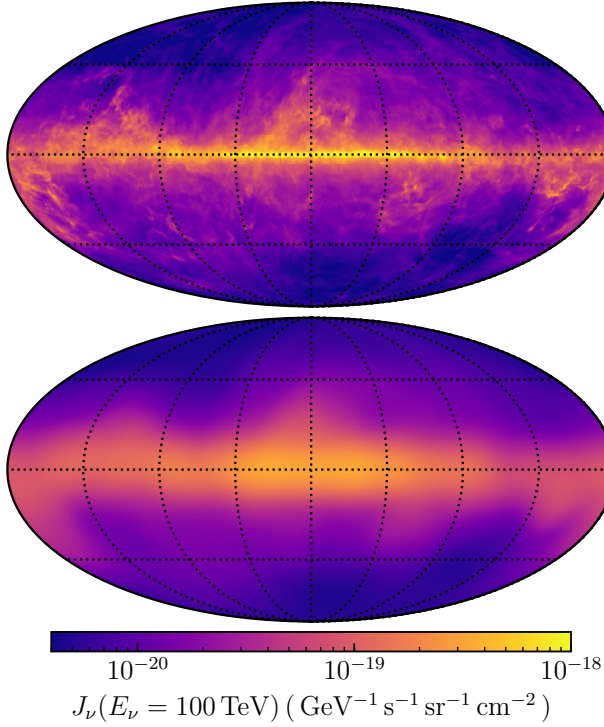


Figure 1. Skymap of the GALPROP predicted Galactic diffuse per-flavour neutrino flux at 100 TeV. The top panel shows the GALPROP predictions for the SA50 source distribution, and the bottom panel is smeared with a $\sigma = 7^\circ$ Gaussian corresponding to the IceCube event uncertainty at 100 TeV.

gas, i.e. $p+p$, $\text{He}+p$, $p+\text{He}$, and $\text{He}+\text{He}$ interactions. The yields for these interactions are computed with **AAfrag202** (Kachelrieß et al. 2019, 2023). While **AAfrag** also includes the yields for $\text{C}+p$, $\text{Al}+p$, and $\text{Fe}+p$ collisions, these heavier species have small relative CR and ISM abundances and so are not included. We calculate the production of the electron and muon neutrinos and antineutrinos (ν_e , ν_μ , $\bar{\nu}_e$, and $\bar{\nu}_\mu$), with the neutrino flux then being computed via a line-of-sight (LoS) integral over the emissivity.

As neutrinos propagate they oscillate between all three possible flavours: ν_e , ν_μ , and ν_τ (Learned & Pakvasa 1994). Over parsec-scale distances the flux of each flavour is expected to be approximately equal (Athar et al. 2000), which has been confirmed in observational results from IceCube Aartsen et al. (2015); Abbasi et al. (2025). The oscillations are not explicitly accounted for in the LoS calculations. As the total all-flavour flux is not altered by the oscillations, we take the per-flavour emission as one third of the total.

3. RESULTS

Figure 1 shows the GALPROP predicted Galactic diffuse per-flavour neutrino emission at the IceCube flux

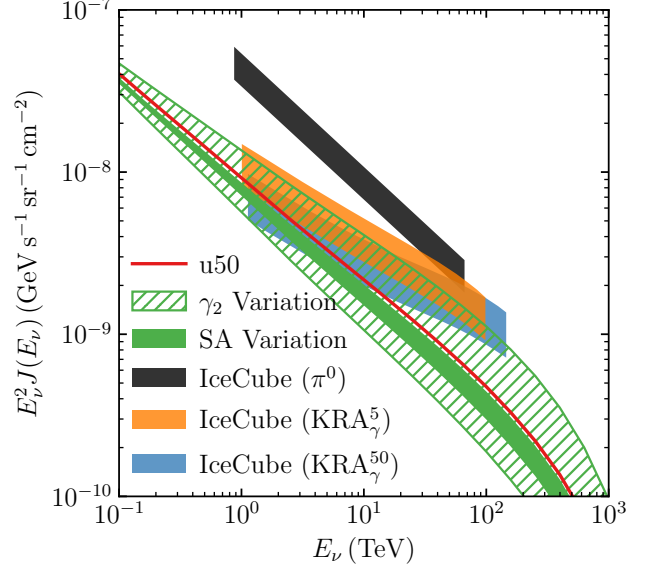


Figure 2. Envelopes of the GALPROP predicted all-sky diffuse per-flavour neutrino flux across the three source distributions (SA variation; green band) and over variations in the injection spectral index (γ_2 variation, green hatched band). Also shown are the three model-dependent IceCube Galactic plane flux measurements (Icecube Collaboration et al. 2023): π^0 (black), KRA_γ^5 (orange), and KRA_γ^{50} (blue).

normalisation energy ($E_\nu = 100$ TeV). In correspondence with the typical event directional uncertainty of IceCube at 100 TeV we also show the GALPROP predictions with a Gaussian blur with a radius of $\sigma = 7^\circ$ (Icecube Collaboration et al. 2023, figure S5). The IceCube collaboration did not publish a skymap of their Galactic neutrino flux, only including a map of the all-sky pre-trial significance for a point-source search. While there is a qualitative spatial agreement between our models and the IceCube neutrino event significance, a quantitative analysis would require using the GALPROP skymap predictions as an input in the IceCube analysis pipeline.

The IceCube detection of the MW plane used machine-learning algorithms to reduce the number of atmospheric neutrino events, increasing the statistics of astrophysical neutrinos by twenty times compared to their previous analysis in Aartsen et al. (2019). Despite this improvement in statistics, IceCube was unable to detect the MW in a blind search and instead relied on spatial models of the Galactic emission to extract the relevant neutrinos. The three neutrino emission models utilised by IceCube are referred to as: π^0 , KRA_γ^5 , and KRA_γ^{50} , where the superscript on the KRA models refers to the cut-off energy of the proton spectrum. These spatial templates are convolved with the detector acceptance and event angular uncertainties, giving event-specific spatial probability density functions that are

then used in a maximum likelihood search. If the Galactic plane is detected with the spatial template, then the model-dependent flux can be computed from the number of observed neutrino events. These model-dependent fluxes take the spectral normalisation as a free parameter that depends on the number of signal events that are spatially correlated with the input models. The IceCube π^0 model is normalised at $E_\nu = 100$ TeV. As the KRA_γ models have a more complex spectral shape and normalisation procedure, their normalisations are quoted only as multiples of their predicted flux (Icecube Collaboration et al. 2023). The three model-dependent IceCube Galactic plane neutrino fluxes are shown in Figure 2 along with our computed range of GALPROP predictions.

We split our GALPROP results into three parts: the u50 flux, and envelopes over the three source distributions (labelled SA variations) and the alterations to the CR injection spectral indices (labelled γ_2 variations). For the changes in the SA models the spread in the envelope is largely due to minor differences in the spectral extrapolation above 1 TeV. While all three SA models and the u50 model have a similar spectral index to that of the IceCube π^0 model, we note that their analysis is not sensitive to the spectral shape of the neutrino emission. The morphology of the Galactic neutrino emission is constant across energies 1–100 TeV for all six of our models.

The IceCube collaboration was unable to resolve any neutrino point sources within the MW. Their neutrino flux therefore represents the total neutrino emission from the Galaxy, i.e. the sum of the diffuse and total source components. The IceCube results in Figure 2 then show the large-scale neutrino emission, i.e. the sum of source components and the diffuse emission. The IceCube Galactic plane neutrino flux is then an upper limit on the hadronic diffuse flux. We expect that the GALPROP predictions, which only includes contributions from the diffuse emission, should underestimate the IceCube large-scale emission. Our GALPROP models shown here underpredict the IceCube results by a factor of ~ 4 , implying that hadronic sources contribute $\sim 75\%$ of the Galactic plane emission.

3.1. Comparison to Gamma-Ray Observatories

The Galactic plane large-scale γ -ray emission has been detected in the VHE energy regime by observatories such as LHAASO (Cao et al. 2023). As the pp collisions create both γ -rays and neutrinos, the two emissions are connected. From Ahlers & Halzen (2017), the γ -ray flux can be converted to a per-flavour neutrino flux via the relation:

$$\frac{1}{3} \sum E_\nu^2 \frac{dN_\nu}{dE_\nu dt}(E_\nu) \approx \frac{1}{2} E_\gamma^2 \frac{dN_\gamma}{dE_\nu dt}(E_\gamma), \quad (1)$$

where the sum is over all neutrino flavours, ν and γ subscripts denotes neutrinos or γ -rays, E is the energy

of the particle, N is the number of particles, and t is time. The neutrino energy is given by $2E_\nu = E_\gamma$, i.e. two times more energy is deposited into the γ -rays than the neutrinos.

For energies above $E_\gamma \approx 40$ TeV ($E_\nu \approx 20$ TeV) the pair absorption of the γ -rays on the background photon fields ($\gamma\gamma \rightarrow e^- e^+$) will reduce the γ -ray flux (Moskalenko et al. 2006; Porter et al. 2018). Pair absorption will therefore lead to an underestimation of the expected neutrino flux from the LHAASO observations. Additionally, there will be contamination from inverse Compton (IC) emission from secondary leptons created in hadronic processes. However, this effect is on the order of 1% of the total emission for a purely hadronic source, and is lower for sources with a primary leptonic component. As the IC emission from secondary leptons is negligible it is not accounted for.

Applying Equation 1 to the LHAASO γ -ray observations provides an upper limit on the expected neutrino emission. This limit assumes no unresolved sources are present in the LHAASO results and a purely hadronic origin of the diffuse emissions. We then construct a lower limit by considering unresolved source estimates from the literature (e.g. Chen et al. 2024; Yan et al. 2024; He et al. 2025; Marinos et al. 2025). Unresolved sources are estimated to account for up to $\sim 75\%$ of the LHAASO emission observed in Chen et al. (2024) for energies below the pair-absorption regime. Within the pair-absorption regime the γ -to- ν conversion given in Equation 1 is invalid.

The neutrino estimates from the LHAASO γ -ray observations are compared to our GALPROP predictions in Figures 3 and 4. Figure 3 shows the upper and lower neutrino flux limits calculated from the LHAASO large-scale γ -ray observations (Cao et al. 2023) for both their ‘inner’ and ‘outer’ analysis regions. Additionally, Figure 4 shows the lower neutrino flux limits calculated from the LHAASO $E_\gamma \geq 5$ TeV (i.e. below the pair-absorption threshold) longitudinal profile from (Chen et al. 2024). These converted LHAASO results are also compared to the u50, SA0, SA50, and SA100 models after applying the LHAASO source masks. For the longitudinal profiles we also applied a $\sigma = 7^\circ$ Gaussian blur to our GALPROP models to matches the IceCube event directional uncertainty, which is also similar to the LHAASO profile longitudinal bin width of 10° .

From both Figures 3 and 4 we see that the diffuse GALPROP neutrino predictions are within the range of estimates computed from the LHAASO γ -ray observations below the pair-absorption regime. The spectral softening in the LHAASO flux (Figure 3) seen above $E_\nu = 20$ TeV ($E_\gamma = 40$ TeV) is not present in our neutrino predictions and is likely due in part to the pair absorption of the γ -ray flux above $E_\gamma \approx 40$ TeV. For the outer Galaxy we find that the GALPROP predictions lie within the upper and lower limits of the converted LHAASO neutrino flux. For the inner region, our GAL-

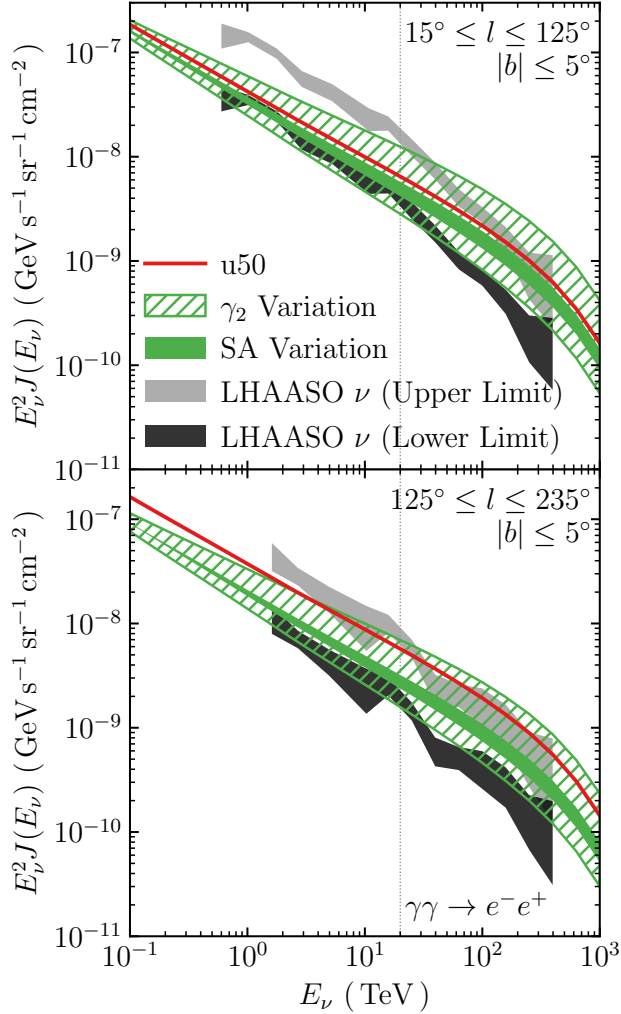


Figure 3. The GALPROP predicted diffuse per-flavour neutrino flux towards to inner (top) and outer (bottom) LHAASO regions across the three source distributions (SA variation; green band) and over variations in the injection spectral index (γ_2 variation, green hatched band). The LHAASO diffuse γ -ray results are shown after converting to expected neutrino fluxes assuming that the emission is 100% hadronic (upper limit, grey) and 25% hadronic (lower limit, black), with the statistical and systematic uncertainties added in quadrature. The vertical dotted line at $E_\nu = 20$ TeV (equivalent to $E_\gamma = 40$ TeV) denotes the region where pair absorption effects reduce the accuracy of the LHAASO γ -to- ν conversion.

PROP predictions lie on the lower limit of the converted LHAASO flux, especially for the model with the softer CR injection index.

The GALPROP results from the three SA source distributions are broadly similar to one another, as expected from previous hadronic γ -ray results (Marinos et al. 2023). The spread between the SA models for

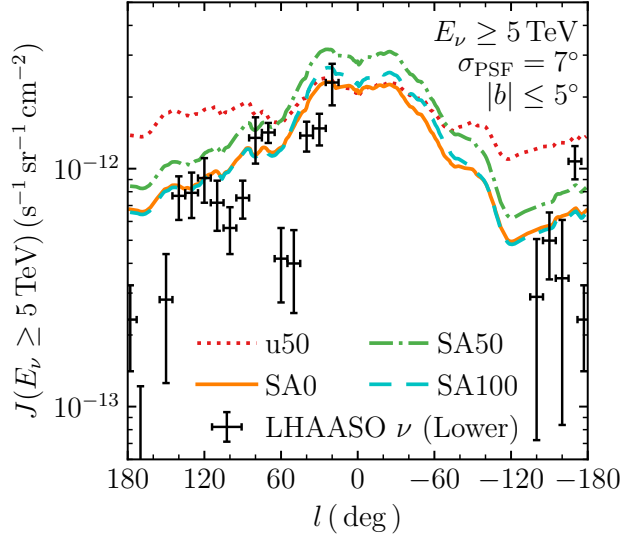


Figure 4. Longitudinal profile taken for $|b| \leq 5^\circ$ of the GALPROP predicted per-flavour neutrino flux at $E_\nu = 100$ TeV across u50 (dotted red), SA0 (solid orange), SA50 (dash-dotted green), and SA100 (dashed cyan) source distributions. The analysis was performed on the skymap with a $\sigma = 7^\circ$ Gaussian smear from Figure 1. Also shown is a lower-bound estimate of the LHAASO data points (black) from (Chen et al. 2024) after converting to a neutrino flux (Equation 1) and subtracting an estimated source component of 75%.

$E_\nu \gtrsim 1$ TeV is largely due to the minor differences in the CR spectral index between the models. Conversely, the uniform CR density model, u50, has an increased flux of CRs in the outer Galaxy compared to the three propagation models due to the increased CR density for Galactic longitudes $|l| \geq 60^\circ$. We find that all three SA models reproduce the general normalisation of the lower limit of the converted LHAASO results for both the inner and outer regions. The situation changes when altering the CR injection spectral index. While the range of GALPROP results are within the uncertainties for the outer region, the softer CR index does not provide a good fit to the LHAASO inner-region results.

Due to the uncertainties in the γ -to- ν flux conversion and the LHAASO large-scale flux estimates we cannot confidently make conclusions on the absolute shape of the longitudinal profiles shown in Figure 4. All three SA source distributions reproduce the general shape of the LHAASO observations, especially for longitudes with smaller uncertainties. The u50 model, which is constructed similarly to the diffuse model used by the LHAASO collaboration, struggles to reproduce the shape of the longitudinal profile beyond $15^\circ \leq |l| \leq 60^\circ$. While the normalisation of the longitudinal profile depends on the spectral index of the GALPROP model,

the shapes of the profiles are independent of the neutrino energy below $E_\nu = 100$ TeV.

4. DISCUSSION

IceCube achieved their neutrino detection of the Galactic plane by forward-folding input models of the expected neutrino flux through the IceCube instrument response functions.² The three input models used in the IceCube analysis were named π^0 , KRA_γ^5 , and KRA_γ^{50} . The IceCube π^0 model is calculated from the pion-decay component of the $S\text{S}^Z4^R20^T150^C5$ GALPROP model³ from Ackermann et al. (2012) and was converted to a neutrino flux via Equation 1. This 13-year-old GALPROP model was optimised for *Fermi*-LAT observations in the GeV regime, and had to be extrapolated to PeV energies (see Icecube Collaboration et al. 2023, supplemental material). The $\text{KRA}_\gamma^{5,50}$ models diffuse CRs using proton cut-off energies 5 and 50 PeV, calculate the neutrino emissivity, then perform line-of-sight integrals to calculate the neutrino emission directly (Gaggero et al. 2015). The updates to the GALPROP framework that we use here allow the computation of the neutrino emission by performing a LoS integral over the neutrino emissivity.

While our predictions are within the observational uncertainties, our results hint towards two potentialities. First, the fraction of unresolved sources could be a function of longitude that increases towards the GC. Second, it is possible that the GALPROP predictions may be underestimating the hadronic emission, particularly towards the GC region. As we have previously shown the total GALPROP γ -ray predictions provide a good description of the LHAASO γ -ray observations (Marinos et al. 2025), any potential alterations must not impact the sum of hadronic and leptonic emissions. We find that a leptonic component is required to reproduce the LHAASO results for all models, including those with harder hadronic injection spectra. However, the large uncertainties in converting between γ -rays and neutrinos, especially in the pair-absorption regime, necessitates future neutrino observations before being utilised to constrain CR diffusion models.

4.1. Unresolved Sources and Leptonic Components

Due to the limited astrophysical neutrino statistics IceCube was unable to resolve point sources within the MW. Hence, the IceCube Galactic plane neutrino flux

is the sum of the diffuse emission with all that from individual sources. The unresolved source component present in the IceCube results does not impact the MW detection as the diffuse emissions are spatially correlated with the VHE/UHE hadronic source emissions. However, this source contamination implies that the number of neutrino events, which dictates the IceCube flux normalisation at $E_\nu = 100$ TeV, is overestimated for the diffuse neutrino flux. The Galactic plane neutrino flux observation is then an upper limit on the true diffuse neutrino flux. Estimating the fraction of emission due to unresolved sources within the MW is required to determine the accuracy of the diffuse models.

Observations from γ -ray experiments can be used to determine the unresolved source component present in the IceCube results. Here we estimate the total source fraction present in the IceCube results we use the LHAASO observations, which cover a similar energy range. However, there are some important caveats for this comparison:

- There is some fraction of leptonic emission present in γ -ray observations. To explain the non-detection of resolved LHAASO sources in the IceCube results, Fang & Halzen (2024) requires that most LHAASO sources have a 20–50% leptonic fraction, i.e. there is a 50–80% hadronic fraction.
- No VHE survey is complete – all diffuse γ -ray observations have their own unresolved source components. Using GALPROP models, He et al. (2025) found that unresolved sources account for 5–27% of the large-scale emission. However, Vecchiotti et al. (2025) claims that the various uncertainties in diffusion models at these energies are too large to conclude on the unresolved source fraction. The results from Yan et al. (2024), which are not based on CR diffusion codes, found that the unresolved emission could contribute as much as 70%.
- Known γ -ray sources may not be completely masked from observations before estimating the ‘diffuse’ emission. We hereafter refer to this as unmasked source emission. Estimates on the fraction of emission from improperly masked/unmasked sources in the LHAASO results range between 0% and 75% of the flux depending on longitude and energy, with higher fractions found towards the GC at 10 TeV (Chen et al. 2024). Our results using updated GALPROP models found that the sum of unmasked and unresolved emission accounts for 50–75% of the LHAASO large-scale emission and has a strong dependence on energy (Marinos et al. 2025). We note that both estimates from Chen et al. (2024) and Marinos et al. (2025) implicitly include a leptonic fraction.

² The IceCube analysis uses the maximum-likelihood technique (Braun et al. 2008), with the input models being denoted S_i in Equation 1 of the supplemental material of Icecube Collaboration et al. (2023).

³ $S\text{S}^Z4^R20^T150^C5$ denotes a GALPROP model that uses a source distribution based on SNRs, a 4 kpc scale height, a radial scale distance of 20 kpc, an atomic hydrogen spin temperature of 150 K, and a magnitude cut applied to the dust map of $E(B - V) = 5$.

- Finally, emission from the γ -ray sources resolved by LHAASO will contribute to the IceCube observations as an unresolved neutrino component. The LHAASO collaboration estimates the resolved source component to account for $\sim 60\%$ of their total large-scale emission (Cao et al. 2023).

The total source contribution to the unmasked LHAASO results is then in the range of 60–90%. The total hadronic source fraction present within the LHAASO results is then in the range of 30–72%. As LHAASO covers the same energy range as IceCube, and as IceCube did not resolve any sources within the MW, the total hadronic fraction for LHAASO should be approximately equal to the unresolved source fraction in the IceCube results. In other words, we expect the unresolved source fraction in IceCube to be equal to 30–72%. Models of the diffuse neutrino emission should then under-estimate the IceCube Galactic plane flux by factors in the range 1.4–3.6 at $E_\nu = 100$ TeV.

For the three SA source distributions, our GALPROP results imply there is a source component in the IceCube results in the range 58–78%, i.e. we underestimate the total Galactic plane flux by factors in the range 2.4–4.6 at 100 TeV. Our results lie on the lower edge of the allowed uncertainty range. Softening the CR injection indices above 100 GeV nuc^{-1} underpredicts the IceCube neutrino flux by a factor ~ 9 at 100 TeV and can be excluded. From the IceCube results we are unable to exclude the harder spectral model. We also find that all of our models require some leptonic component to reproduce the LHAASO observations.

The older GALPROP model utilised in the IceCube analysis ($^{SSZ}4^R20^T150^C5$, from Ackermann et al. 2012) underpredicts the IceCube emission by a factor of ~ 4.5 . Our current best-fit GALPROP models (SA0, SA50, and SA100) shown in Figure 2 underpredict the IceCube per-flavour neutrino emission by a factor ~ 4 . While both the old and our updated GALPROP models are within the range of expected values, the difference to the flux reproduction is due to the improved CR flux measurements that provide a more accurate extrapolation to TeV–PeV energies compared to the older models (Porter et al. 2017).

Our GALPROP flux results lie on the lower limit obtained from the IceCube uncertainties. While the models are within the range of factors expected from source estimates, it could hint towards a mismatch between the models and observations. Either there is a hadronic CR source component lying on the upper edge of our expectations, there is some mismodelling, or some combination of both. Understanding the exact dynamics requires future observations with increased neutrino statistics, as well as an analysis of the sensitivity of the IceCube methods to the spectral shape of the input models.

5. SUMMARY

The detection of the Galactic plane in neutrinos by IceCube is an important step towards understanding the origin of CRs, providing a constraint on the hadronic component of the γ -ray emission. These results have motivated the inclusion of neutrinos in the GALPROP framework. In this work we investigated the new neutrino predictions computed from updated GALPROP models and made comparisons to the IceCube flux.

IceCube did not have enough statistics to detect the Galactic plane in a blind search, and relied on input models of the expected neutrino emission. As no localised source component is subtracted from their results, the IceCube flux is an upper limit on all neutrino emission within the MW (i.e. both individual sources and the diffuse emission). The presence of this source component must be considered to prevent overfitting of diffusion simulation results to the data. From VHE/UHE γ -ray experiments, we find that the source fraction for the IceCube neutrino flux is likely in the range of 30–72%. Diffuse neutrino emission models should then underestimate the IceCube total flux by factors in the range 1.4–3.6. The updated GALPROP models investigated here are within this uncertainty range, underestimating the IceCube total Galactic plane neutrino flux by factors 2.4–4.6.

The significance of the IceCube detection of the Galactic plane depends on the input model (KRA_γ^{50} ; 3.96σ , KRA_γ^5 ; 4.37σ , and GALPROP-based π^0 ; 4.71σ). The KRA_γ models have a worse spatial agreement with the observations compared to the GALPROP-based model, resulting in a lower significance for a detection of the MW. The models presented here have an improved agreement with the IceCube flux normalisation and have recently been shown to agree with TeV γ -ray results from both H.E.S.S. (Marinos et al. 2023) and LHAASO (Marinos et al. 2025). Hence, we expect their use in the IceCube analysis pipeline will increase the neutrino detection significance for the MW. However, strict limits on the diffuse hadronic fraction within the Galactic plane will not be possible until future observations are obtained.

For further constraints on the neutrino flux we also use the >10 TeV γ -ray observations from LHAASO as a proxy measurement of the neutrino emission. We convert the LHAASO large-scale γ -ray results to an upper-limit neutrino flux, and then compute the lower-limit by taking source estimates available throughout the literature. Five of our six GALPROP models fit within this range. Hence, we find that the current GALPROP models reproduce both the observed Galactic plane neutrino flux from IceCube and the estimates calculated from LHAASO, within the experimental uncertainties of the observatories. We also find that the large-scale emission results from LHAASO requires some leptonic component in all cases. We do not require any changes

to our fundamental assumptions on particle injection, transport, cross sections, the ISM distributions, or the inclusion of dark matter, to reproduce the current observations of the Galactic plane γ -ray or neutrino emission.

ACKNOWLEDGMENTS

GALPROP development is partially funded via NASA grants 80NSSC22K0477, 80NSSC22K0718, and 80NSSC23K0169. CR data was compiled via the Cosmic-Ray Data Base (CRDB) (Maurin et al. 2014, 2020, 2023). We thank S. Sclafani for guidance on interpreting the IceCube results and K. Fang for useful discussions.

AUTHOR CONTRIBUTIONS

PDM was responsible for the analysis and writing of the manuscript. TAP, IVM obtained the funding and edited the manuscript. GJ, GPR edited the manuscript.

Software: astropy (Astropy Collaboration et al. 2013, 2018), GALPROP (Moskalenko & Strong 1998; Strong & Moskalenko 1998; Porter et al. 2022), HEALPix (Górski et al. 2005), matplotlib (Hunter 2007), numpy (Harris et al. 2020), and scipy (Virtanen et al. 2020).

6. APPENDIX

We fit our CR injection spectra such that the propagated flux agrees with local observations at 100 GeV, and extrapolate to higher energies (see Marinos et al. 2023). Given the uncertainties in the >10 TeV regime, we test a range of spectral indices for the injected CRs for rigidities $R > 266$ GV. The spectral indices are denoted $\gamma_{2,p}$ and $\gamma_{2,He}$ for protons and helium, respectively. We show the GALPROP propagated CR proton and helium spectra for the SA50 source distribution at the Solar location along with local data in Figures 5 and 6.

REFERENCES

Aartsen, M. G., Ackermann, M., Adams, J., et al. 2015, *PhRvL*, 114, 171102, doi: [10.1103/PhysRevLett.114.171102](https://doi.org/10.1103/PhysRevLett.114.171102)

Aartsen, M. G., Ackermann, M., Adams, J., et al. 2019, *ApJ*, 886, 12, doi: [10.3847/1538-4357/ab4ae2](https://doi.org/10.3847/1538-4357/ab4ae2)

Abbasi, R., Ackermann, M., Adams, J., et al. 2025, arXiv e-prints, arXiv:2510.24957, doi: [10.48550/arXiv.2510.24957](https://doi.org/10.48550/arXiv.2510.24957)

Abeysekara, A. U., Alfaro, R., Alvarez, C., et al. 2019, *ApJ*, 871, 96, doi: [10.3847/1538-4357/aaf5cc](https://doi.org/10.3847/1538-4357/aaf5cc)

Ackermann, M., Ajello, M., Atwood, W. B., et al. 2012, *ApJ*, 750, 3, doi: [10.1088/0004-637X/750/1/3](https://doi.org/10.1088/0004-637X/750/1/3)

Adriani, O., Akaike, Y., Asano, K., et al. 2022, *PhRvL*, 129, 101102, doi: [10.1103/PhysRevLett.129.101102](https://doi.org/10.1103/PhysRevLett.129.101102)

Adriani, O., Akaike, Y., Asano, K., et al. 2023, *PhRvL*, 130, 171002, doi: [10.1103/PhysRevLett.130.171002](https://doi.org/10.1103/PhysRevLett.130.171002)

Aguilar, M., Ali Cavasonza, L., Ambrosi, G., et al. 2021, *PhR*, 894, 1, doi: [10.1016/j.physrep.2020.09.003](https://doi.org/10.1016/j.physrep.2020.09.003)

Ahlers, M., & Halzen, F. 2017, *Progress of Theoretical and Experimental Physics*, 2017, 12A105, doi: [10.1093/ptep/ptx021](https://doi.org/10.1093/ptep/ptx021)

Alemanno, F., An, Q., Azzarello, P., et al. 2021, *PhRvL*, 126, 201102, doi: [10.1103/PhysRevLett.126.201102](https://doi.org/10.1103/PhysRevLett.126.201102)

An, Q., Asfandiyarov, R., Azzarello, P., et al. 2019, *Science Advances*, 5, eaax3793, doi: [10.1126/sciadv.aax3793](https://doi.org/10.1126/sciadv.aax3793)

Astropy Collaboration, Robitaille, T. P., Tollerud, E. J., et al. 2013, *A&A*, 558, A33, doi: [10.1051/0004-6361/201322068](https://doi.org/10.1051/0004-6361/201322068)

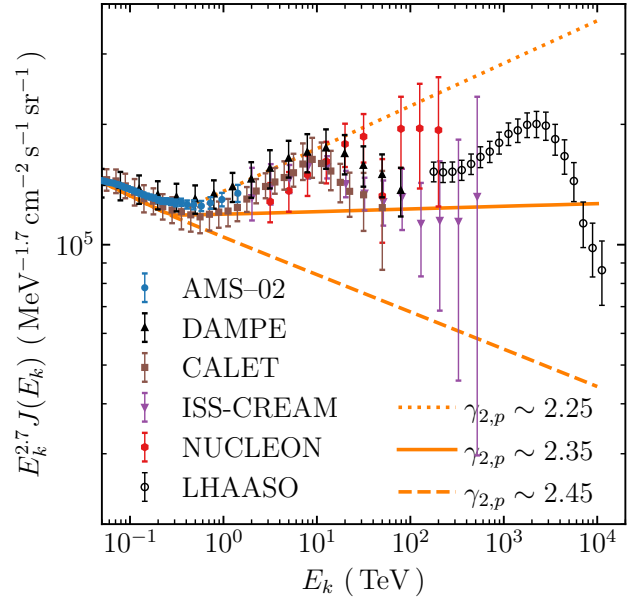


Figure 5. Proton kinetic energy spectrum above 50 GeV at the Solar location. The GALPROP propagated spectrum is shown for three values of the highest-energy injection index. Observational datapoints are from AMS-02 (blue circles; Aguilar et al. 2021), DAMPE (black triangles; An et al. 2019), CALET (brown squares; Adriani et al. 2022), ISS-CREAM (purple triangles; Choi et al. 2022), NUCLEON (red hexagons; Grebenyuk et al. 2019), and LHAASO (black circles; The LHAASO Collaboration et al. 2025).

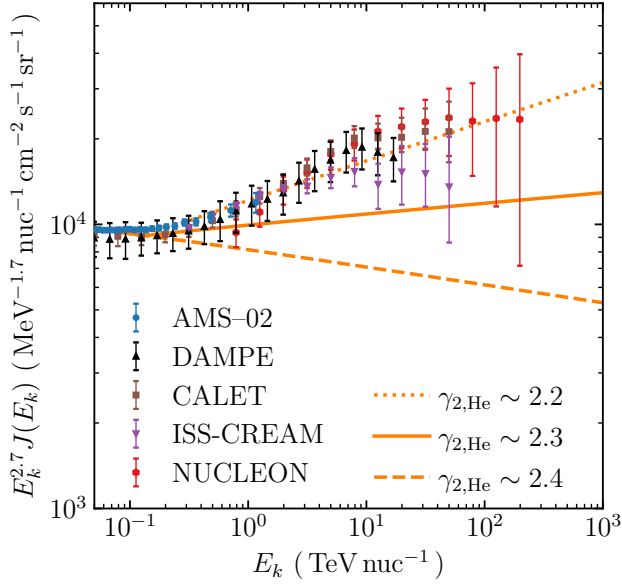


Figure 6. Helium kinetic energy spectrum above 50 GeV at the Solar location. The GALPROP propagated spectrum is shown for three values of the highest-energy injection index. Observational datapoints are from AMS-02 (blue circles; Aguilar et al. 2021), DAMPE (black triangles; Alemanno et al. 2021), CALET (brown squares; Adriani et al. 2023), CREAM-I+III (purple triangles; Yoon et al. 2017), and NUCLEON (red hexagons; Grebenyuk et al. 2019).

Astropy Collaboration, Price-Whelan, A. M., Sipőcz, B. M., et al. 2018, AJ, 156, 123, doi: [10.3847/1538-3881/aabc4f](https://doi.org/10.3847/1538-3881/aabc4f)

Athar, H., Jeżabek, M., & Yasuda, O. 2000, PhRvD, 62, 103007, doi: [10.1103/PhysRevD.62.103007](https://doi.org/10.1103/PhysRevD.62.103007)

Bhadra, S., Thoudam, S., Nath, B. B., & Sharma, P. 2025, ApJ, 989, 74, doi: [10.3847/1538-4357/ade796](https://doi.org/10.3847/1538-4357/ade796)

Boschini, M. J., Della Torre, S., Gervasi, M., et al. 2020, ApJS, 250, 27, doi: [10.3847/1538-4365/aba901](https://doi.org/10.3847/1538-4365/aba901)

Braun, J., Dumm, J., De Palma, F., et al. 2008, Astroparticle Physics, 29, 299, doi: [10.1016/j.astropartphys.2008.02.007](https://doi.org/10.1016/j.astropartphys.2008.02.007)

Cao, Z., Aharonian, F., An, Q., et al. 2023, PhRvL, 131, 151001, doi: [10.1103/PhysRevLett.131.151001](https://doi.org/10.1103/PhysRevLett.131.151001)

Chen, E.-S., Fang, K., & Bi, X.-J. 2024, Chinese Physics C, 48, 115105, doi: [10.1088/1674-1137/ad72d4](https://doi.org/10.1088/1674-1137/ad72d4)

Choi, G. H., Seo, E. S., Aggarwal, S., et al. 2022, ApJ, 940, 107, doi: [10.3847/1538-4357/ac9d2c](https://doi.org/10.3847/1538-4357/ac9d2c)

Fang, K., Bi, X.-J., & Yin, P.-F. 2020, ApJ, 903, 69, doi: [10.3847/1538-4357/abb8d7](https://doi.org/10.3847/1538-4357/abb8d7)

Fang, K., & Halzen, F. 2024, Journal of High Energy Astrophysics, 43, 140, doi: [10.1016/j.jheap.2024.07.001](https://doi.org/10.1016/j.jheap.2024.07.001)

Gaggero, D., Grasso, D., Marinelli, A., Urbano, A., & Valli, M. 2015, ApJL, 815, L25, doi: [10.1088/2041-8205/815/2/L25](https://doi.org/10.1088/2041-8205/815/2/L25)

Górski, K. M., Hivon, E., Banday, A. J., et al. 2005, ApJ, 622, 759, doi: [10.1086/427976](https://doi.org/10.1086/427976)

Grebenyuk, V., Karmanov, D., Kovalev, I., et al. 2019, Advances in Space Research, 64, 2546, doi: [10.1016/j.asr.2019.10.004](https://doi.org/10.1016/j.asr.2019.10.004)

Harris, C. R., Millman, K. J., van der Walt, S. J., et al. 2020, Nature, 585, 357, doi: [10.1038/s41586-020-2649-2](https://doi.org/10.1038/s41586-020-2649-2)

He, J., Zeng, H., Zhang, Y., et al. 2025, ApJ, 980, 17, doi: [10.3847/1538-4357/ada6b2](https://doi.org/10.3847/1538-4357/ada6b2)

Hunter, J. D. 2007, Computing in Science & Engineering, 9, 90, doi: [10.1109/MCSE.2007.55](https://doi.org/10.1109/MCSE.2007.55)

IceCube Collaboration, Aartsen, M. G., Ackermann, M., et al. 2018a, Science, 361, 147, doi: [10.1126/science.aat2890](https://doi.org/10.1126/science.aat2890)

IceCube Collaboration, Aartsen, M. G., Ackermann, M., et al. 2018b, Science, 361, eaat1378, doi: [10.1126/science.aat1378](https://doi.org/10.1126/science.aat1378)

IceCube Collaboration, Abbasi, R., Ackermann, M., et al. 2022, Science, 378, 538, doi: [10.1126/science.abg3395](https://doi.org/10.1126/science.abg3395)

Icecube Collaboration, Abbasi, R., Ackermann, M., et al. 2023, Science, 380, 1338, doi: [10.1126/science.adc9818](https://doi.org/10.1126/science.adc9818)

Jóhannesson, G., Porter, T. A., & Moskalenko, I. V. 2018, ApJ, 856, 45, doi: [10.3847/1538-4357/aab26e](https://doi.org/10.3847/1538-4357/aab26e)

Jóhannesson, G., Porter, T. A., & Moskalenko, I. V. 2019, ApJ, 879, 91, doi: [10.3847/1538-4357/ab258e](https://doi.org/10.3847/1538-4357/ab258e)

Kachelrieß, M., Moskalenko, I. V., & Ostapchenko, S. 2019, Computer Physics Communications, 245, 106846, doi: [10.1016/j.cpc.2019.08.001](https://doi.org/10.1016/j.cpc.2019.08.001)

Kachelrieß, M., Ostapchenko, S., & Tjemsland, J. 2023, Computer Physics Communications, 287, 108698, doi: [10.1016/j.cpc.2023.108698](https://doi.org/10.1016/j.cpc.2023.108698)

Learned, J. G., & Pakvasa, S. 1994, arXiv e-prints, hep, doi: [10.48550/arXiv.hep-ph/9408296](https://doi.org/10.48550/arXiv.hep-ph/9408296)

Liu, W., Guo, Y.-Q., & Yuan, Q. 2019, JCAP, 2019, 010, doi: [10.1088/1475-7516/2019/10/010](https://doi.org/10.1088/1475-7516/2019/10/010)

Malkov, M. A., & Moskalenko, I. V. 2021, ApJ, 911, 151, doi: [10.3847/1538-4357/abe855](https://doi.org/10.3847/1538-4357/abe855)

Malkov, M. A., Moskalenko, I. V., Diamond, P. H., & Cao, M. 2024, Advances in Space Research, 74, 4264, doi: [10.1016/j.asr.2024.08.060](https://doi.org/10.1016/j.asr.2024.08.060)

Marinos, P. D., Porter, T. A., Rowell, G. P., Jóhannesson, G., & Moskalenko, I. V. 2025, ApJ, 981, 93, doi: [10.3847/1538-4357/adadfb](https://doi.org/10.3847/1538-4357/adadfb)

Marinos, P. D., Rowell, G. P., Porter, T. A., & Jóhannesson, G. 2023, MNRAS, 518, 5036, doi: [10.1093/mnras/stac3222](https://doi.org/10.1093/mnras/stac3222)

Maurin, D., Dembinski, H. P., Gonzalez, J., Mariş, I. C., & Melot, F. 2020, Universe, 6, 102, doi: [10.3390/universe6080102](https://doi.org/10.3390/universe6080102)

Maurin, D., Melot, F., & Taillet, R. 2014, *A&A*, 569, A32, doi: [10.1051/0004-6361/201321344](https://doi.org/10.1051/0004-6361/201321344)

Maurin, D., Ahlers, M., Dembinski, H., et al. 2023, European Physical Journal C, 83, 971, doi: [10.1140/epjc/s10052-023-12092-8](https://doi.org/10.1140/epjc/s10052-023-12092-8)

Moskalenko, I. V., Porter, T. A., & Strong, A. W. 2006, *ApJL*, 640, L155, doi: [10.1086/503524](https://doi.org/10.1086/503524)

Moskalenko, I. V., & Strong, A. W. 1998, *ApJ*, 493, 694, doi: [10.1086/305152](https://doi.org/10.1086/305152)

Moskalenko, I. V., Strong, A. W., Ormes, J. F., & Potgieter, M. S. 2002, *ApJ*, 565, 280, doi: [10.1086/324402](https://doi.org/10.1086/324402)

Orlando, E., & Strong, A. 2013, *MNRAS*, 436, 2127, doi: [10.1093/mnras/stt1718](https://doi.org/10.1093/mnras/stt1718)

Porter, T. A., Jóhannesson, G., & Moskalenko, I. V. 2017, *ApJ*, 846, 67, doi: [10.3847/1538-4357/aa844d](https://doi.org/10.3847/1538-4357/aa844d)

Porter, T. A., Jóhannesson, G., & Moskalenko, I. V. 2022, *ApJS*, 262, 30, doi: [10.3847/1538-4365/ac80f6](https://doi.org/10.3847/1538-4365/ac80f6)

Porter, T. A., Moskalenko, I. V., Strong, A. W., Orlando, E., & Bouchet, L. 2008, *ApJ*, 682, 400, doi: [10.1086/589615](https://doi.org/10.1086/589615)

Porter, T. A., Rowell, G. P., Jóhannesson, G., & Moskalenko, I. V. 2018, *PhRvD*, 98, 041302, doi: [10.1103/PhysRevD.98.041302](https://doi.org/10.1103/PhysRevD.98.041302)

Pshirkov, M. S., Tinyakov, P. G., Kronberg, P. P., & Newton-McGee, K. J. 2011, *ApJ*, 738, 192, doi: [10.1088/0004-637X/738/2/192](https://doi.org/10.1088/0004-637X/738/2/192)

Robitaille, T. P., Churchwell, E., Benjamin, R. A., et al. 2012, *A&A*, 545, A39, doi: [10.1051/0004-6361/201219073](https://doi.org/10.1051/0004-6361/201219073)

Strong, A. W., & Moskalenko, I. V. 1998, *ApJ*, 509, 212, doi: [10.1086/306470](https://doi.org/10.1086/306470)

Strong, A. W., Moskalenko, I. V., & Reimer, O. 2000, *ApJ*, 537, 763, doi: [10.1086/309038](https://doi.org/10.1086/309038)

Strong, A. W., Moskalenko, I. V., & Reimer, O. 2004, *ApJ*, 613, 962, doi: [10.1086/423193](https://doi.org/10.1086/423193)

Strong, A. W., Orlando, E., & Jaffe, T. R. 2011, *A&A*, 534, A54, doi: [10.1051/0004-6361/201116828](https://doi.org/10.1051/0004-6361/201116828)

The LHAASO Collaboration, Cao, Z., Aharonian, F., et al. 2025, arXiv e-prints, arXiv:2505.14447. <https://arxiv.org/abs/2505.14447>

Vecchiotti, V., Peron, G., Amato, E., et al. 2025, *JCAP*, 2025, 041, doi: [10.1088/1475-7516/2025/09/041](https://doi.org/10.1088/1475-7516/2025/09/041)

Virtanen, P., Gommers, R., Oliphant, T. E., et al. 2020, *Nature Methods*, 17, 261, doi: [10.1038/s41592-019-0686-2](https://doi.org/10.1038/s41592-019-0686-2)

Yan, K., Liu, R.-Y., Zhang, R., et al. 2024, *Nature Astronomy*, 8, 628, doi: [10.1038/s41550-024-02221-y](https://doi.org/10.1038/s41550-024-02221-y)

Yoon, Y. S., Anderson, T., Barrau, A., et al. 2017, *ApJ*, 839, 5, doi: [10.3847/1538-4357/aa68e4](https://doi.org/10.3847/1538-4357/aa68e4)